JOURNAL OF MATERIALS SCIENCE 30 (1995) 3475–3482

Thermochemical synthesis and characterization of nanostructured chromium silicide and silicon carbide composite materials

P. LUO, P. R. STRUTT
Connecticut Advanced Technology Center for Precision Manufacturing and Department of Metallurgy, University of Connecticut, Storrs, CT 06269, USA

Nanostructured chromium silicide/silicon carbide in the form of composite powders have been synthesized from water-soluble precursors by a spray-dry and thermal conversion process. Two materials compositions were investigated to provide insight into the relation between the initial precursor composition and the composition of the synthesized nanostructured materials. The multiphase materials that were produced contain (i) cubic β-SiC and hexagonal $Cr_{5-X}Si_{3-Y}C_{X+Y}(Cr_5Si_3C_X)$. A systematic study of the chemical and structured nature of these materials during and after processing was carried out using thermogravimetric analysis, differential thermal analysis, inductively coupled plasma spectrometry, Fourier transform–infrared spectroscopy, and X-ray diffractometry analysis. The calculated average grain size is around 20–80 nm. Microstructure observation using scanning electron microscopy and transmission electronmicroscopy revealed a distribution of nanoparticles with dimensions in the range 10–100 nm. This is in agreement with the precalculation from an analysis of X-ray line broadening.

1. Introduction

Recent scientific discoveries show that materials can display particularly novel mechanical, electrical, magnetic and other properties when particle or grain diameters are of nanometre dimensions. Specific examples include nanostructured or nanocomposite materials possessing high hardness combined with improved fracture toughness [1–3] and high degree of homogeneity by constructing nanophases to improve the local properties of materials [4]. These features clearly show the potential advantages of exploiting the properties of designed nanostructured composite materials in advanced technology applications.

In high-temperature mechanical property applications where composite materials are required to have superior strength combined with enhanced fracture toughness, phase selection is normally restricted, because limited ductility or inherently brittle phases may not be used. Nanostructured composite materials, however, provide a way for overcoming this limitation, and now it is possible, for example, to develop a composite where a nanoscale dispersion of silicon carbide particles strengthen an intermetallic silicide matrix. In considering the constituent phases, it is noted that intermetallic silicides are currently used for electric furnace elements, structural components, protective coatings and large-scale integration devices [5–7]. This is because of their metal-like resistivities, very good oxidation resistance, high strength, and high-temperature stability. Silicon carbide is a preferred reinforcing phase [7, 8] in metal silicide/silicon carbide composites because of its high elastic modulus, high thermal conductivity, small thermal expansion coefficient, high-temperature strength, and excellent thermal shock resistance. Furthermore, its semiconducting properties may possibly lead to interesting discoveries in the electric properties of metal silicide/silicon carbide nanostructured composites.

In view of the basic scientific interest and technological relevance of nanostructured intermetallic silicide dispersion-strengthened composite materials, a study has been initiated for synthesizing and characterizing a selected system. This paper presents new results in synthesizing a chromium silicide matrix material, dispersion strengthened by nanoscale silicon carbide particles. Based on newly developed synthesis technologies at the University of Connecticut in the last few years [9–12], a solution chemical synthesis route is selected for synthesizing a chromium silicide and silicon carbide nanocomposite. The approach involves (i) the spray drying of water-soluble inorganic compounds to form an intermediate precursor, and (ii) thermo-chemical conversion of the intermediate precursor to form the final product material at an elevated temperature in a dynamic gas environment.

2. Experimental procedure

Chromium chloride ($CrCl_3 \cdot 6H_2O$), sodium methylsiliconate ($Ch_3Si(ONa)_3$) with 30 wt % water and dextrose (D-glucose $C_6H_{12}O_6$) were dissolved in distilled water to produce an aqueous solution where the

0022–2461 © *1995 Chapman & Hall*

molar ratio was 1:2:2 or 1:4:2. Spray drying of the precursor was performed in a spray drier. The solution was pumped from a feed tank into the spray nozzle. Atomization was achieved using compressed air. The resulting powder was cyclone separated from the flowing gas stream. The intermediate precursor powders were placed in an alumina crucible in a tube furnace. The system was cyclically evacuated to 10^{-3} torr (1 torr = 133.322 Pa) and flushed with argon gas several times, and then back-filled with argon gas to near ambient pressure. During this process, the system was maintained under an argon flow rate of 100 ml min^{-1} and an elevated temperature for 5 h.

Various characterization technologies were applied to study the precursors, intermediate and final composites. Thermogravimetric analysis (TGA) and differential thermal analysis (DTA) were performed using a simultaneous high-temperature TGA/DTA analyser under a argon flow for 5 h. This process is in the condition similar to the synthesis environment except the heating rate. Structural analysis of precursors, intermediate and final composites versus processing temperatures were performed using X-ray diffractometry (XRD) and Fourier transform–infrared spectroscopy (FT–IR). Morphologies of the final composites were revealed by scanning electron microscopy (SEM) and transmission electron microscopy (TEM). The average particle sizes of constituent phases were calculated from X-ray spectra and revealed by TEM. Particle-size distribution of agglomerated particles and their particulates were conducted by image analysis. Chemical composition analysis was performed by inductively coupled plasma spectrometry (ICP).

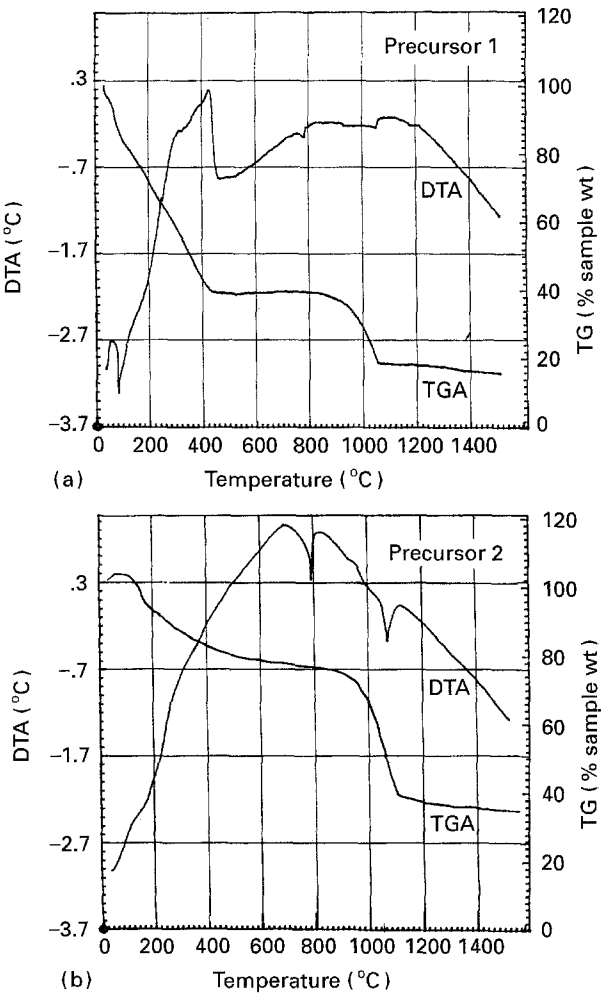

Figure 1 Thermogravimetric analysis (TGA) and differential thermal analysis (DTA) for (a) precursor 1 and (b) precursor 2.

3. Characterization and discussion

3.1. TGA/DTA analysis

In the TGA/DTA measurement, two precursors, named precursor 1 (1:2:2) and precursor 2 (1:4:2), were examined. As shown in Fig. 1, both precursors (see TGA curves) first start to lose water at 80 °C and undergo a decomposition in the 100–400 °C temperature range with a total weight loss of 60% for precursor 1 and 20% for precursor 2. The weight losses for the two precursors in the temperature range from 100–400 °C are mainly due to water vaporization and dextrose ($C_6H_{12}O_6$) decomposition in the precursor. The second major weight losses for the two precursors take place in the 800–1020 °C temperature range. They are due to the vaporization of NaCl. Precursor 1 has a relatively higher percentage of the dextrose than precursor 2, therefore the first weight loss plateau for precursor 1 is much lower than for precursor 2. Precursor 2 contains a higher percentage (twice that in precursor 1) of sodium methylsiliconate, therefore the TGA curve of precursor 2 drops at a rate which is twice that of precursor 1. This result is shown in TGA curves by weight percentages dropping from 80% to 40% for precursor 2 and from 40% to 20% for precursor 1. Finally, it reaches to a total loss of around 60% for precursor 2 and 80% for precursor 1.

DTA curves provide information of the various phase formations with the processing temperatures if the phase transformation releases or absorbs heat. A peak can be observed when the temperature difference between the sample and the reference is changed. From the DTA analysis results, it has been determined that precursor 1 has phase formations at 440 °C, which is an exothermic reaction, and at 780 and 1100 °C, which are endothermic reactions. These reactions were investigated by X-ray analysis. They will be described in Section 3.4. The phase formations are identified as chromium oxide at 440 °C, chromium silicide and silicon carbide at 780 °C, and simultaneous silicon oxide and sodium chloride vaporization at 1080 °C. Precursor 2 has the phase formations of chromium silicide and silicon carbide at 780 °C, and simultaneous silicon dioxide and sodium chloride vaporization at 1080 °C (same as precursor 1). In precursor 2, phase formation of chromium oxide at 440 °C is not observed. Silicon carbide formation by conversion of silicon oxide and carbon graphite at 1250 °C for both precursors is not observed either, but this reaction in both precursors is determined by the X-ray analysis (see Fig. 6, Section 3.4). The explanation is not clear but it indicates at least that the heat flow of the formation of silicon carbide nanocrystallites from silicon dioxide and carbon graphite is too low to be detected here.

3.2. ICP analysis

Inductively coupled plasma elementary spectrometry (ICP) was used to analyse the samples which were made at different processing temperatures for 5 h. Sample powders were dissolved in the HF, HCl and HNO_3 concentrated solutions in a Teflon vessel and placed in a microwave for 10 min. Chromium, sodium and silicon compounds were dissolved completely into the solution under a high pressure. The undissolved powder was carbon graphite. The solution containing elemental chromium, sodium and silicon was injected into the ICP and the weight percentages of each element were determined. The carbon concentration was determined by weighing the undissolved powder remaining. Fig. 2 shows the analytical results for elemental sodium. Sodium concentration drops sharply from near 100 wt % to around 2 wt % in the temperature range between 600 and 1000 °C. This analytical result supports the TGA result well. In fact, the theoretical melting point of sodium chloride is at 804 °C. Beyond this melting point, sodium chloride will vaporize under the continuous argon flow.

Analytical results of elemental chromium, silicon and carbon in the temperature range from 900–1300 °C are plotted in Fig. 3. The relation of concentrations versus temperatures can be calculated into a linear relationship using the linear regression method

$$C_C = -0.05858\,T + 106.9314 \quad (1)$$

$$C_{Si} = 0.02262\,T - 2.35846 \quad (2)$$

$$C_{Cr} = 0.03746\,T - 17.0963 \quad (3)$$

where C_C, C_{Si}, and C_{Cr} represent the concentration of elemental carbon, silicon and chromium; T is the processing temperature (°C). Summing Equations 1–3 gives

$$C_{sum} = 0.0015\,T + 87.4766 \quad (4)$$

where C_{sum} represents the total concentration of these three elements.

The slope of Equation 1 is almost equal to the addition of the slopes of Equations 2 and 3. This result indicates that the increase in chromium and silicon concentrations is mainly due to the decrease of carbon concentration. The slope of Equation 3 is slightly greater than Equation 2. This might be due to a small loss of elemental silicon in the formation of silicon monoxide gas [13]. The sum of the constants of the above three equations is equal to 87.5% instead of 100%, because of the 2 wt % Na impurity as NACl (in total about 5 wt %) and the loss of silicon monoxide (SiO).

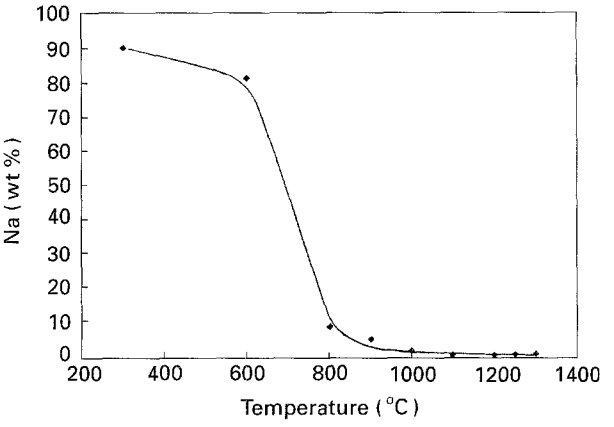

Figure 2 Chemical analysis (ICP) of sodium concentration versus processing temperatures.

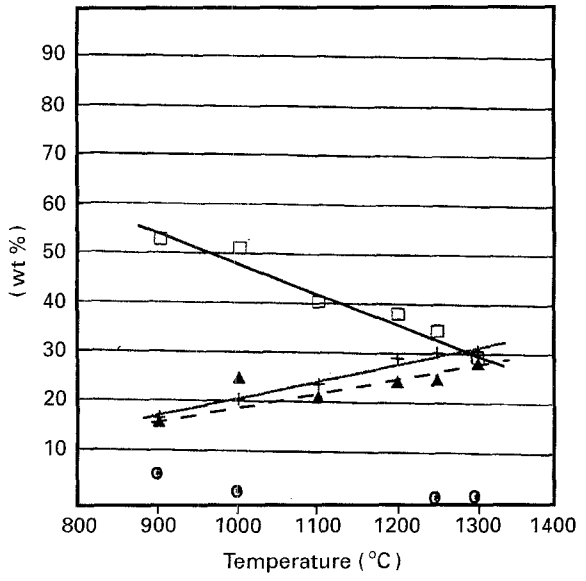

Figure 3 Chemical analysis (ICP) of (+) chromium, (▲) silicon, sodium (◑) and (□) carbon weight percentages versus processing temperatures in the range 900–1300 °C.

3.3. FT–IR analysis

FT–IR analysis provides information about the bond formation regardless of crystalline or amorphous phases. Precursor 1 was mixed with KBr, pressed into a thin disc and analysed in the transmission mode. Fig. 4 shows the results of FT–IR analysis. The spectra of sodium methylsiliconate and D–(+)–glucose (dextrose) [14] exhibit the complexity by

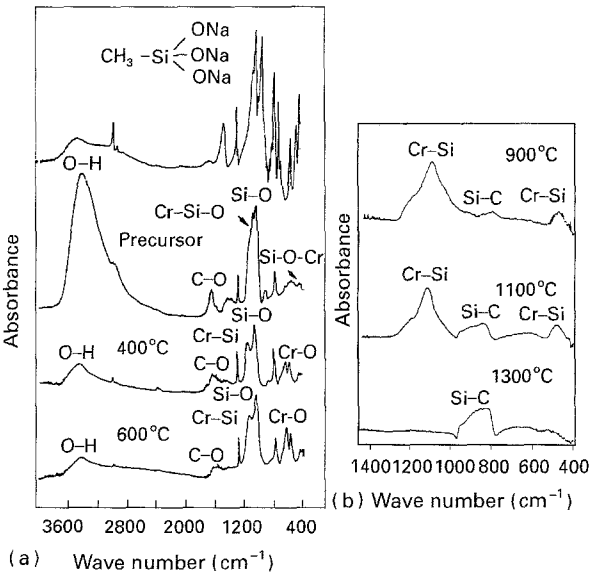

Figure 4 (a, b) Fourier transform–infrared spectroscopy analysis for the investigation of bond structures versus processing temperatures.

revealing many peaks in the wave numbers range 400–2000 cm^{-1}. After chromium chloride was added, the spectrum was changed. The starting materials were not as individual substances existing in the precursor but reacted to form a new complex compound. The elemental chromium, silicon and carbon in the molecular range mixed very well so that the condition for forming the nanostructured final product was satisfied. The precursor spectrum indicated that the precursor contained Si–O, C–O, and O–H bonds at wave number 1100, 1600 and 3500 cm^{-1}, respectively. Stretching of elemental chromium to the Si–O bond, represented as the Cr–Si–O, bond was observed. Another stretching of elemental silicon to the Cr–O bond, represented as the Si–O–Cr bond, was also found.

By increasing the processing temperatures, absorbencies of the O–H and C–O groups were significantly reduced. Up to 600 °C, water and organic groups, which have low melting points, were vaporized and decomposed. Si–O–Cr and Cr–Si–O bonds decomposed into Cr–O and Cr–Si bonds which were detected at wave numbers 580, 630 and 1150 cm^{-1}. On continually increasing the temperature to 900, 1100 and 1300 °C, chromium silicides and silicon carbides such as Cr–Si and Si–C bonds were found to be the only strong peaks appearing in the spectra, which are at the wave numbers 1150 and 844 cm^{-1}. A smaller amount of the Si–O bond (at wave number 1100 cm^{-1}) could not be determined because of the very broad Cr–Si and Si–C peaks. At 900 °C, the relatively higher absorbence of Cr–Si to Si–C bond was obtained. At 1300 °C, the absorbence of the Si–C bond is very strong compared with the Cr–Si bond; therefore, it could not be found. Chromium silicide and silicon carbide powders purchased from JM and CERAC were used as standard materials to support above analytical results (Fig. 5). The shape of the

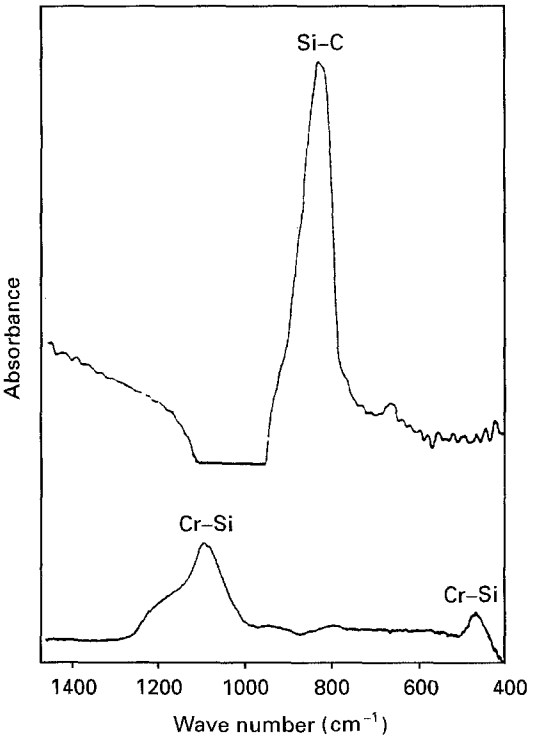

Figure 5 Fourier transform–infrared spectroscopy analysis for the standard chromium silicide and silicon carbide made by JM and CERAC.

Cr–Si peak in the synthesized material is the same as in the standard material, but not the Si–C peak. This is broadened compared with the standard spectrum of SiC with a sharp peak.

3.4. X-ray analysis

X-ray diffraction analysis provides detailed information of the crystalline structural characteristics (crystalline phase formations). Fig. 6 shows the X-ray

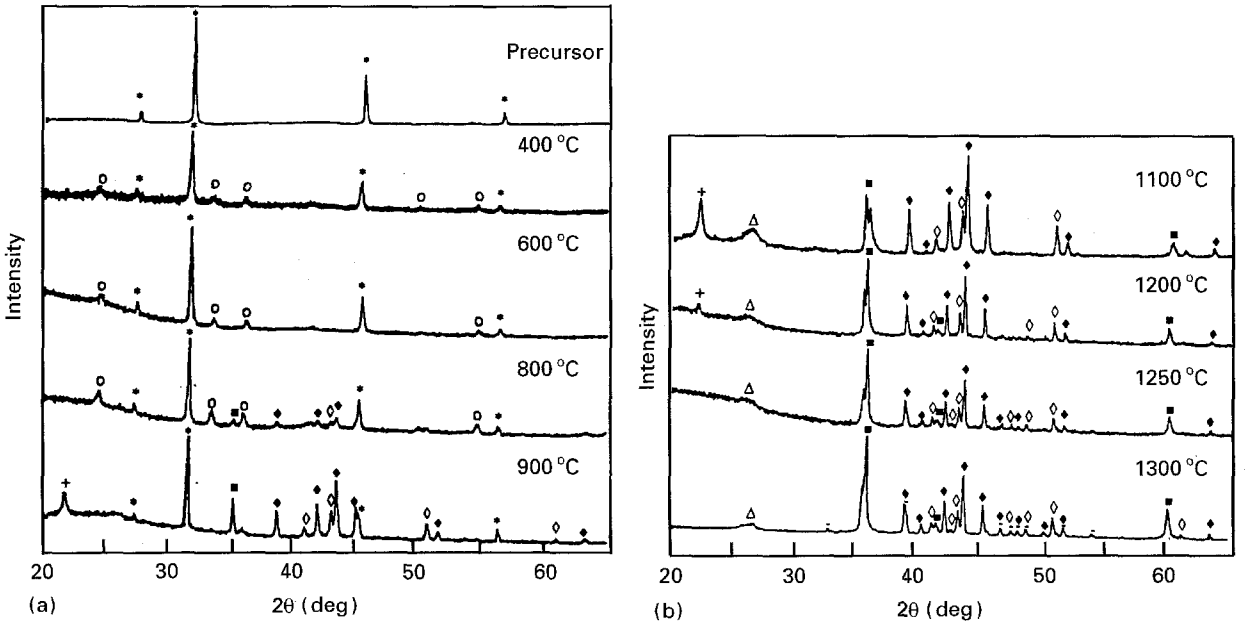

Figure 6 (a, b) X-ray diffraction patterns for the samples which were performed at elevated temperatures for the investigation of chemical reactions and phase formations during the synthesis process. (■) SiC, (+) SiO_2, (○) Cr_2O_3, (*) NaCl, (◇) $CrSi_2$, (◆) Cr_5Si_3, (△) C, (—) Cr_3C_2.

spectra for the samples from precursor 1 which were processed at different temperatures. The precursor contains NaCl crystalline phase with an amorphous phase, which is a complex of elemental chromium, silicon and carbon. By increasing the processing temperature to 400 °C, Cr_2O_3 crystalline phase started to form. Cr_2O_3 crystalline phase grew continually up to 800 °C and was converted into chromium silicide at 900 °C. The chromium silicide formation can be explained by chromium oxide and silicon oxide reacting with the existing carbon, which was decomposed from dextrose at 400 °C [15], into chromium silicides and silion carbide [15, 16]. These reactions are described as follows

$$Cr_2O_3 + 4SiO_2 + \frac{69}{5}C \rightarrow \frac{2}{5}Cr_5Si_3 (+ CrSi_2) + \frac{14}{5}SiC + 11CO \quad (5)$$

The formation of chromium disilicide in the final product from precursor 1 (appearing as a small peak next to the major Cr_5Si_3 peak in the X-ray spectrum) was observed, but not from precursor 2.

With continually increasing temperature, sodium chloride began to vaporize from 900 °C and was complete at 1200 °C. There was only about 2 wt % Na remaining in the final product as an impurity, which has been already discussed (Section 3.2).

Silicon dioxide cristobalite crystallized at 900 °C and grew at 1100 °C. At 1250 °C, silicon dioxide was reduced to β-SiC by reaction with carbon. Fig. 7 shows that the relative percentage of silicon carbide increased and that of silicon dioxide decreased. The chemical reactions [13] may be described as

$$SiO_2 + C \rightarrow SiO + CO \quad (6)$$

$$SiO + 2C \rightarrow SiC + CO \quad (7)$$

The above reactions occur at 1250 °C under an argon flow. the pressure of SiO (g) in the reaction was determined directly by analysis of the sublimate condensed in the colder part of the furnace. The following mechanism of SiO_2 reduction is suggested [13]

$$SiO_2 \xrightarrow{C} SiO \xrightarrow{C} SiC \quad (8)$$

Compared with the commercial methodology to produce β-SiC from silica reacted with coke at 1600 °C [17], this synthesis route provides excellent economic aspects for producing pure nanostructured β-SiC product by leaching out chromium compounds with HCl. Up to 1300 °C, partial chromium silicides were reacted with the excess carbon to form Cr_3C_2 and β-SiC.

The precursor concentration ratio of chromium, silicon and carbon plays an important role in the phase formations (this will be discussed in a subsequent paper using a ternary phase diagram). Precursor 1 at 1250 °C is converted into β-SiC, Cr_5Si_3, and $CrSi_2$, with certain amount of excess carbon. Precursor 2 at 1250 °C is converted to $Cr_{5-X}Si_{3-Y}C_{X+Y}$ ($Cr_5Si_3C_X$) and β-SiC (Fig. 8). The $Cr_{5-X}Si_{3-Y}C_{X+Y}$ ($Cr_5Si_3C_X$) phase was named T-phase in the work of

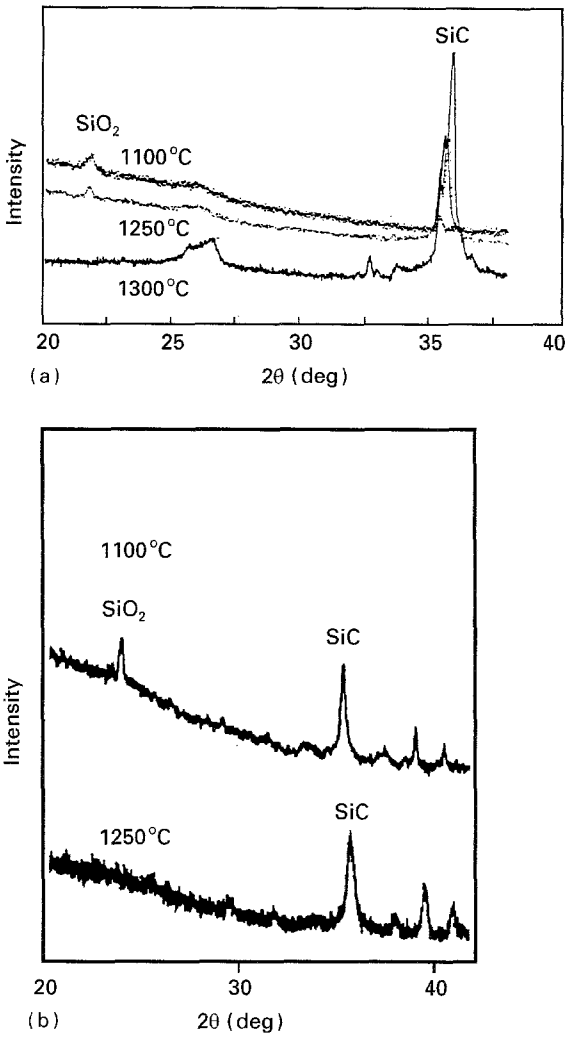

Figure 7 (a, b) Silicon carbide formation from the reduction of silicon dioxide by carbon graphite. (a) 1:2:2 precursor 1, (b) 1:4:2 precursor 2.

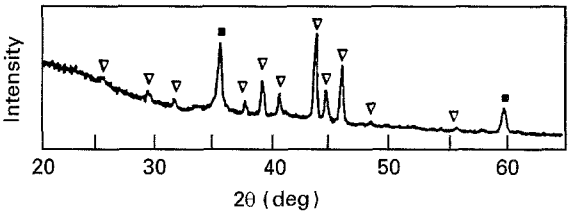

Figure 8 X-ray characterization of the final product from 1:4:2 precursor 2 at 1250 °C for 5 h. (▽) $Cr_{5-X}Si_{3-Y}C_{X+Y}$, (■) SiC.

Pellegrini *et al.* [18]. The stoichiometry range was found to be $Cr_{5\pm0.2}Si_{3\pm0.1}C_X$ with $0.25 < X < 1.05$. The wide compositional ranges of the T-phase were also observed by Parthe *et al.* [19] and J. van den Boomgaard [20].

3.5. Particle-size characterization

3.5.1. Average particle size calculation from the X-ray peak broadening effect

X-ray peak broadening is a result of the refinement of the microcrystalline size and the internal strain. The full widths at half maximum of the Bragg peaks, ΔK, are plotted as a function of their K-values. The line

TABLE I Grain size calculation from X-ray patterns

Precursor	Temperature	d (nm)		
	(°C)	SiC	Cr_5Si_3	$Cr_{5-x}Si_{3-y}C_{x+y}$
1	900	51	76.4	–
	1100	24.7	27.5	–
	1200	25.4	–	–
	1250	28.7	–	–
	1300	25.9	65.5	–
	1400	35.1	–	–
	1500	27.8	–	–
2	1250 °C (5 h)	163	–	35.4

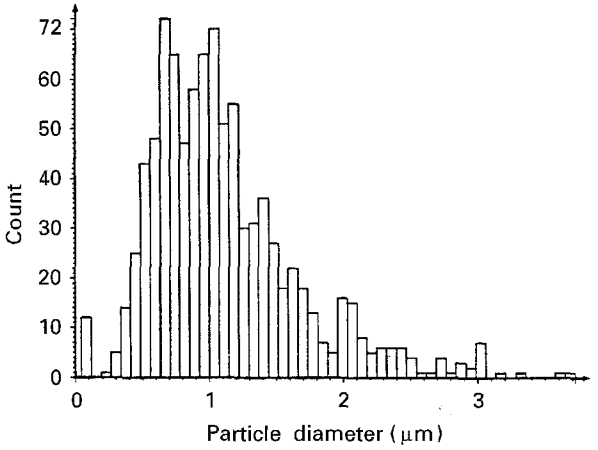

Figure 9 Histogram of the agglomerated particle-size distribution.

broadening, which is due to the small crystal size and internal strain, is given by [21]

$$\Delta K = 0.9(2\pi/d) + A\langle e^2\rangle^{1/2} \quad (9)$$

where d is the crystal size, A is a constant that depends on the strain distribution and is approximately equal to 1 for a random distribution of dislocations, and $\langle e^2\rangle^{1/2}$ is the root mean square (r.m.s.) strain which is neglected here for powder analysis. The microcrystalline size calculated from Equation 9 is shown in Table I. There is no significant temperature effect on the crystalline sizes. They are in the range 20–100 nm.

3.5.2. Particle-size distribution on agglomerated particles and their particulates

Image analysis was applied to investigate the particle-size distribution. A scanning electron micrograph of the agglomerated composite powder was taken and input into a image analyser. The diameters of these particles were measured on the screen and statistically calculated. Fig. 9 shows the size distribution of the agglomerated particles which were produced from precursor 2 at 1250 °C for 5 h. The agglomerated particles have the average (mean) size of 1.12 μm. The maximum size is 3.72 μm and the minimum size is 0.0438 μm. Of the measured particles, 90% are in the size range below 2 μm. It is difficult to measure the minimum particle size because very tiny particles which are below 0.1 μm are not possible to count from the scanning electron micrograph.

In order to analyse the particulates of the agglomeration, sample powders which were produced from precursor 2 at 1250 °C for 5 h were analysed using high-resolution TEM. Fig. 10 shows the size distribution of the particulate. The average (mean) value of the size is 50.47 nm, the maximum value is 92 nm. The minimum value is 13.6 nm. The particulate-size distribution is in the type of a Gaussian distribution.

3.6. Electron microscopy examinations

SEM and TEM were used to examine the morphology of the particles. There are small particulates contained in the large particles which have a diameter of about 2 μm (Fig. 11a). The particles show transparent and hollow structures under the electron beam. To confirm this characteristic, sample preparation for the

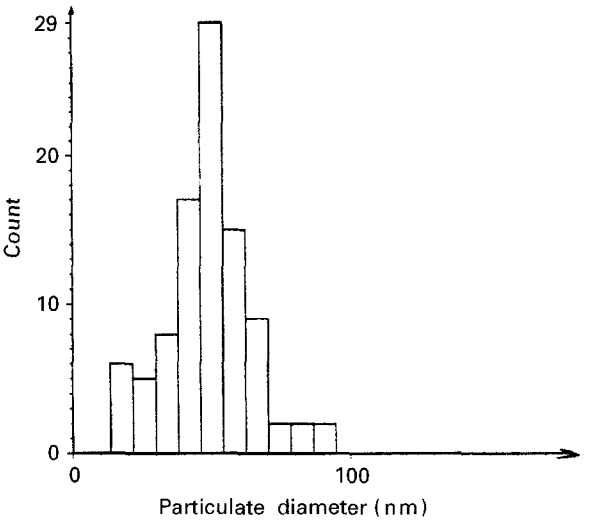

Figure 10 Histogram of the unagglomerated particulate-size distribution.

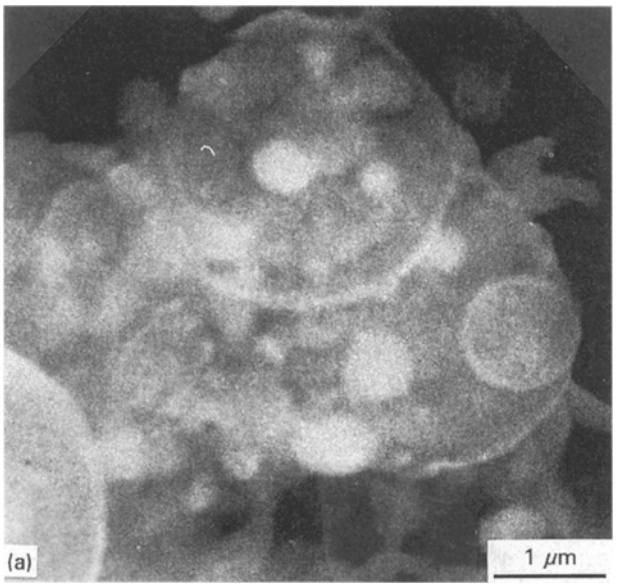

Figure 11 (a) High-resolution scanning electron microscopy (SEM) examination showing the agglomerated composite particle with the electron-transparent morphology. (b) Scanning electron microscopy (SEM) examination showing the agglomerated composite particle with the hollow structure.

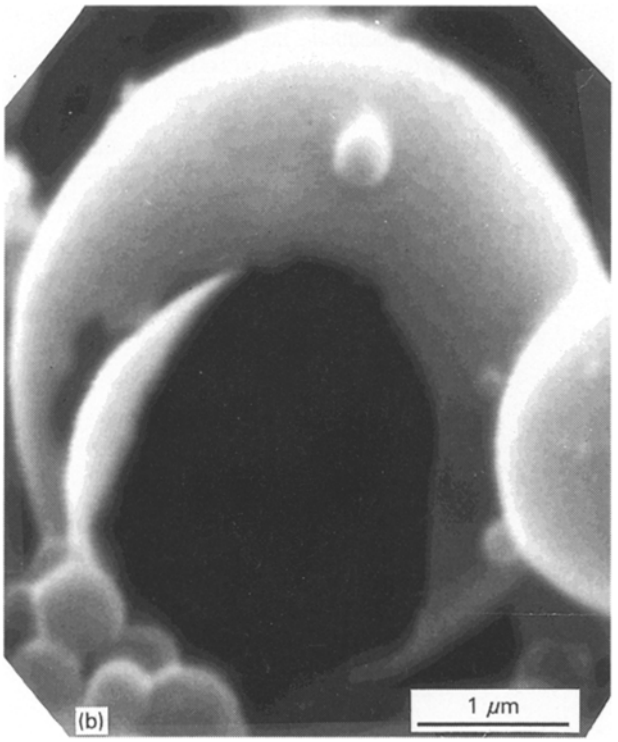

Figure 11 (Continued)

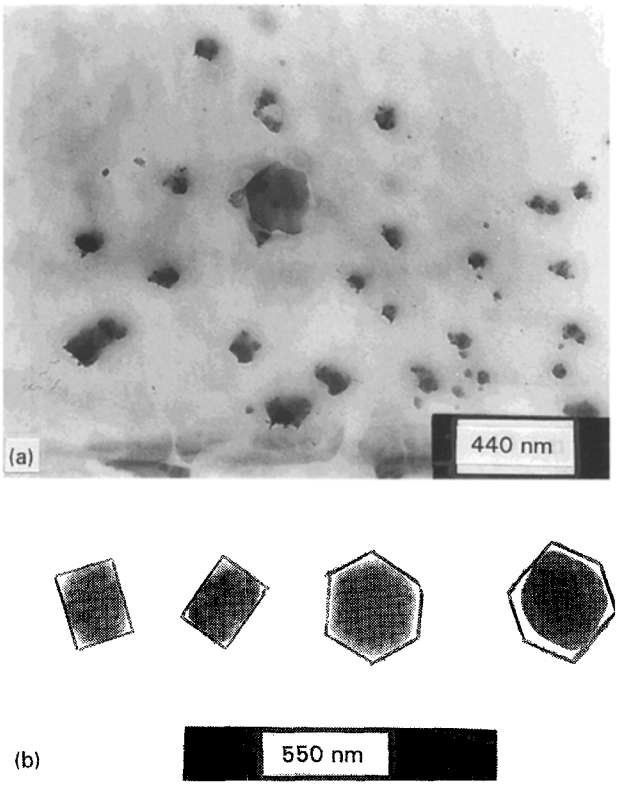

Figure 12 (a, b) Transmission electron microscopy (TEM) bright-field images showing the size and the shape of particulate.

SEM study was specially done by compressing powder particles on a substrate to somehow break the shell of the particle. Fig. 11b shows a broken particle with the empty feature inside. The reason for the formation of the hollow particle might be due to the precursor preparation by initial spray drying. The spray-dried precursor particles were examined and were also found to similar hollow structures (see [12], Fig. 1).

The particulates were observed under the TEM. Fig. 12 shows the unagglomerated particulate with cubic and hexagonal structures. They are single nanocrystallites.

4. Conclusion

A chemical synthesis route utilizing spray drying has been developed to prepare materials with compositional and structural uniformity on the nanoscale level and in bulk quantity. A new precursor has been developed for the first time to synthesize nanostructured chromium silicide–silicon carbide composite. The synthesis process is analysed and discussed. The oxide formation is the intermediate step in the formation of silicides and carbides in this synthesis process. The synthesis reaction route can be summarized as follows

$$CH_3Si(ONa)_3 + CrCl_3 + C_6H_{12}O_6 \xrightarrow{\text{Spray dry}}$$

$$\text{Precursor powder} \xrightarrow{<800^\circ C} Cr_2O_3 + SiO_2 + C$$

$$\xrightarrow{1250\,^\circ C} Cr_5Si_3C_X + SiC + CO \qquad (10)$$

Composites of chromium silicide in various modifications with β-SiC can be designed by changing the precursor Cr:Si:C ratio. Solution concentrations of chromium, silicon and carbon are 1:2:2 and 1:4:2; the corresponding final products are tetragonal Cr_5Si_3, hexagonal $CrSi_2$ and cubic β-SiC, and hexagonal $Cr_{5-X}Si_{3-Y}C_{X+Y}$ ($Cr_5Si_3C_X$) and cubic β-SiC. The theoretical grain size of the constituent phases are calculated from the X-ray line broadening and are between 20 and 80 nm. The composite powder finally synthesized is agglomerated into the spherical hollow shape. Agglomerated particulates are found by TEM to show cubic and hexagonal shapes. TEM examination and particulate-size distribution reveal that the particulates are in the same size range of 10–100 nm, with a mean value 50.47 nm, which agrees with the calculated values from the X-ray line broadening.

References

1. R. W. SIEGEL, S. RAMASAMY, H. HAHN, Z. LI, T. LU, R. GRONSKY, *J. Mater. Res.* **3** (1988) 1376.
2. R. ROY, in "Material Research Society Symposia Proceedings," Vol. 286, edited by S. Konarneni, J. C. Parker and G. J. Thomas (Materials Research Society, Pittsburgh, PA, 1993) p. 241.
3. J-P. HIRVONEN, R. LAPPALAINEN, H. KATTELUS, J. LIKONEN, I. SUNI, H. KUNG, T. R. JERVIS and M. NASTASI, *ibid.*, p. 373.
4. P. LUO. P. R. STRUTT and T. D. XIAO, *Mater. Sci. Eng.* **B17** (1993) 126.
5. H. MOISSAN, "The Electric Furnace" (Edward Arnold, London, 1904).
6 S. P. MURARKA, "Silicides for VLSI applications" (Academic Press, London, 1983).
7. A. K. VASUDEVAN and J. J. PETROVIC, *Mater. Sci. Eng.* **A155** (1992) 1.
8. W. S. GIBBS, J. J. PETROVIC and R. E. HONNELL, *Ceram. Eng. Sci. Proc.* **8** (1987) 645.

9. K. E. GONSALVES, P. R. STRUTT, T. D. XIAO and P. G. KLEMENS, *J. Mater. Sci.* **27** (1992) 3231.
10. T. D. XIAO, K. E. GONSALVES, P. R. STRUTT and P. G. KLEMENS, *ibid.* **28** (1993) 1334.
11. T. D. XIAO, Y. D. ZHANG, P. R. STRUTT. J. I. BUDNICK, K. MOHN and K. E. KONSALVES, *J. Nanostruct. Mater.* **2** (1993) 285.
12. P. LUO and P. R. STRUTT, in "Materials Research Society Symposia Proceedings", Vol. 286, edited by S. Konarneni, J. C. Parker and G. J. Thomas (Materials Research Society, Pittsburgh, PA, 1993) p. 185.
13. W. POCH and A. DIETZEL, *Ber. Deut. Keram. Ges.* **39** (1962) 413/26.
14. C. J. POUCHERT, "The Aldrich Library of Infrared Spectra", 3rd Edn (Adrich Chemical Company, Inc., Milwaukee, WN, Wisconsin).
15. H. MOISSAN, *Compt. Rend.* **121** (1895) 621/6, 624 (or G. MAEHLING, Handbook, Si).
16. G. DE CHALMOT, *Am. Chem. J.* **19** (1897) 69/70 (or G. MAEHLING, Handbook, Si).
17. SHIGEYUKI SOMIYA and YOSHIZO INOMATA, "Silicon carbide ceramics" (Elsevier Applied Science, London, New York, 1991).
18. P. W. PELLEGRINI, B. C. GIESSEN and J. M. FELDMAN, *Solid State Sci. Technol.* **119** April (1972) 535.
19. E. PARTHE, H. SCHACHNER and H. NOWOTNY, *Monat. Chem.* **86** (1958) 182.
20. J. VAN DEN BOOMGAARD, *Philips Res. Rept* **23** (1968) 270.
21. T. D. SHEN, K. Y. WANG, M. X. QUAN and J. T. WANG, *J. Mater. Sci. Lett.* **11** (1992) 1576.

Received 7 January
and accepted 4 October 1994